ENVIRONMENTAL RESEARCH
LETTERS

PURPOSE-LED PUBLISHING™ Part of the ENVIRONMENTAL RESEARCH SERIES

LETTER • OPEN ACCESS

Permafrost thaw affects the chemistry of mountain ponds

To cite this article: N Colombo *et al* 2025 *Environ. Res. Lett.* **20** 094007

ENVIRONMENTAL RESEARCH
LETTERS

LETTER

Permafrost thaw affects the chemistry of mountain ponds

N Colombo[1,*], M Pettauer[2], S Brighenti[3,4], D Godone[5], F Salerno[6], R Balestrini[7], C A Delconte[7], E Pintaldi[1], A Benech[1], L Paro[8], M Martin[1], A Brunier[9], N Guyennon[10] and M Freppaz[1]

[1] University of Turin, Department of Agricultural, Forest and Food Sciences, Grugliasco, Italy
[2] Institute of Applied Geosciences, Graz University of Technology, Graz, Austria
[3] Competence Centre for Mountain Innovation Ecosystems, Free University of Bozen/Bolzano, Bolzano, Italy
[4] Eco Research, Bolzano, Italy
[5] Research Institute for Geo-Hydrological Protection, National Research Council of Italy, IRPI-CNR Torino, Italy
[6] Institute of Polar Sciences, National Research Council of Italy, ISP-CNR Milano, Italy
[7] Water Research Institute, National Research Council of Italy, IRSA-CNR Brugherio, Italy
[8] Department Natural and Environmental Risks, Environmental Protection Agency of Piemonte Region, Torino, Italy
[9] Climate Change Unit, Environmental Protection Agency of Valle d'Aosta, Saint-Christophe, Italy
[10] Water Research Institute, National Research Council of Italy, IRSA-CNR Montelibretti, Italy
[*] Author to whom any correspondence should be addressed.

E-mail: nicola.colombo@unito.it

Keywords: sulfide oxidation, water quality, mountains, European Alps, cryosphere, LTER

Supplementary material for this article is available online

OPEN ACCESS

RECEIVED
18 April 2025

REVISED
8 July 2025

ACCEPTED FOR PUBLICATION
15 July 2025

PUBLISHED
1 August 2025

Abstract

Permafrost is warming and thawing due to climate change. Among the related effects, water quality modification has gained increasing attention globally. Nevertheless, the impacts of diffuse permafrost thaw on water chemistry in high-mountain areas remain largely unexplored. Here, we investigated the seasonal and interannual variability of water chemistry of two close-by ponds located in high-elevation catchments (European Alps, NW Italy) with and without permafrost. We analyzed major ions and stable water isotopes (2014–2022; weekly to monthly sampling during the ice-free season) and leveraged ground thermal measurements in a 30-m deep borehole. We also used geochemical modeling to investigate the impacts of permafrost thaw on dominant weathering processes. Despite similar climatic conditions, lithological characteristics, and water sources contribution, we observed higher concentrations and more pronounced seasonal increases of most solutes in the pond located within the permafrost catchment compared to the pond in the permafrost-free catchment. This was particularly evident for sulfate, with mean concentrations approximately four times higher in the permafrost pond. In the permafrost catchment, progressive warming and thawing during the investigation period enhanced sulfide oxidation, likely due to increased exposure of unweathered, sulfide-bearing rock particles. However, enhanced weathering did not lead to acidification and water quality deterioration due to pH buffering capacity provided by dissolving silicates and carbonates. Global warming is expected to further accelerate permafrost thawing and related chemical weathering in transitional permafrost areas. Water quality issues may arise in catchments with poor acid neutralizing potential of rocks.

1. Introduction

Global permafrost is warming [1, 2] and the active layer is deepening [3] due to anthropogenic climate change [4]. As a consequence, the effects of permafrost thaw are occurring worldwide [5] and affect climate [e.g. 6], infrastructure stability [e.g. 7], hydrology [e.g. 8], and ecosystems [e.g. 9].

Although underreported with respect to other impacts, and mostly investigated in latitudinal permafrost environments, permafrost thaw can deeply influence the chemistry of freshwater systems [9, 10]. Indeed, following permafrost thaw, increasing concentrations of major ions and trace elements can occur due to: (i) deepening of flow pathways, which enhances the interactions between water and ground

subsurface, (ii) thickening of the active layer and melting of near surface, solute-rich ground ice, and (iii) increasing contribution of deep, highly mineralized groundwater [11]. These processes can concur in deteriorating the water quality, mostly due to enhanced sulfide oxidation [12–14].

In mountain areas, most research has focused on the impacts of permafrost thaw on slope instability [e.g. 15, 16] and the acceleration/destabilization of permafrost-related landforms such as rock glaciers [e.g. 17, 18]. For these landforms, an increasing number of studies have highlighted the effects of permafrost thaw and ground-ice melt on water chemistry. Despite growing evidence that permafrost thaw can deeply degrade water quality, most of our knowledge on mountain areas derives from rock glacier-fed systems [e.g. 19, 20], whereas the possible impact of diffuse permafrost thaw on water chemistry has received little attention [e.g. 21, 22].

Here, we investigated the seasonal and interannual variability of water chemistry of two ponds located at high elevation (>2800 m a.s.l.) in the European Alps (NW Italy). To do this, we took advantage of a unique dataset composed of nine years (2014–2022) of major ions and stable water isotopes observations, collected from weekly to monthly during the ice-free season. We then leveraged ground thermal measurements in a 30-m deep borehole to characterize the permafrost dynamics. Finally, we exploited geochemical modelling to investigate the main weathering processes occurring in the studied settings.

Our goal is to disentangle the impacts of mountain permafrost thaw on water chemistry, taking advantage of the comparison of two close-by lentic systems located in catchments with and without permafrost.

2. Materials and methods

2.1. Field sites description

The investigated ponds are located in the long term ecological research (LTER) site Angelo Mosso Scientific Institute (https://deims.org/17210eba-d832-4759-89fa-9ff127cbdf6e), in the Western Italian Alps (Monte Rosa massif, figure 1): Bowditch Pond (hereafter: Permafrost Pond – PermaP; 2900 m a.s.l.) and Cimalegna Pond (hereafter: No Permafrost Pond – NoPermaP; 2800 m a.s.l.).

The catchments of the ponds have quasi-identical climatic conditions (supplement, text S1), given their close proximity (linear distance ca. 500 m), but differ in terms of cryospheric conditions. Indeed, permafrost is present in the PermaP catchment, mostly on the north-facing slopes of the Corno del Camoscio peak (3024 m a.s.l., figure 1), and it is absent in the NoPermaP catchment [23].

The bedrock of both catchments is mainly composed of micaschists, with gneisses and amphibolites that are mostly present in the PermaP catchment, and few quartzite outcrops that occur in the NoPermaP catchment; minor inclusions of carbonate-rich rocks occur in the area [23]. The land cover of the PermaP catchment is dominated by coarse debris deposits, while fine sediment/soil (mostly vegetated) is the main land cover type in the NoPermaP catchment (table 1) [23, 24].

2.2. Permafrost and snow measurements

To analyze the permafrost thermal dynamics, we used ground temperature data from a 30-m deep borehole located close to the southern border of the PermaP catchment at 3020 m a.s.l. (figure 1). The borehole was drilled mostly in the bedrock, with only a few-decimeter-thin layer of fine-grained material covering the surface. The thermistor chain is composed of 25 sensors (supplement, text S2). We retrieved continuous data from 1 October 2013 to 30 September 2023. Some technical issues occurred at the station, such as lightning strikes, thus we selected ground temperature series at five depths (4.7, 9.6, 17.5, 26.5, 29.4 m) having fewer missing values and representative of ground thermal dynamics at the site (supplement, text S2). For these depths, we calculated the decadal warming rates of the annual mean ground temperatures (MGTs) using ordinary least squares linear regression [cf. 25].

Given the importance of snowmelt in determining intra- and interannual concentration variations in high-elevation water [25–27], we estimated the snowpack duration using two approaches with different spatial and temporal resolution. (i) To provide an estimate of the snow-covered area in the catchments, we applied a spatially-distributed approach based on remote sensing analysis, using the Landsat 8 Operational Land Imager imagery (30-m spatial resolution; supplement, text S3). (ii) To monitor the local snowpack melt progression, we used daily data on snow thickness from an automatic weather station (AWS) located close to the ponds (Col d'Olen AWS, 2900 m a.s.l., figure 1).

Remote sensing analyses showed that snow-cover dynamics were similar in the two catchments in the period of the first sampling of each season, with snow-cover values mostly at 0 % (table S1). Thus, given the similar snow-cover conditions, for each sampling date at both ponds we calculated the variable days after snowmelt (DAS), based on the melt-out date of snow obtained from the Col d'Olen AWS. We used this as a proxy to describe the seasonal patterns of water isotopic and chemical characteristics, while accounting for the contrasting end of the snowmelt period among different years [see 26, 27].

2.3. Field sampling

We collected water samples from both ponds when water surfaces were ice-free, between 2014 and 2022

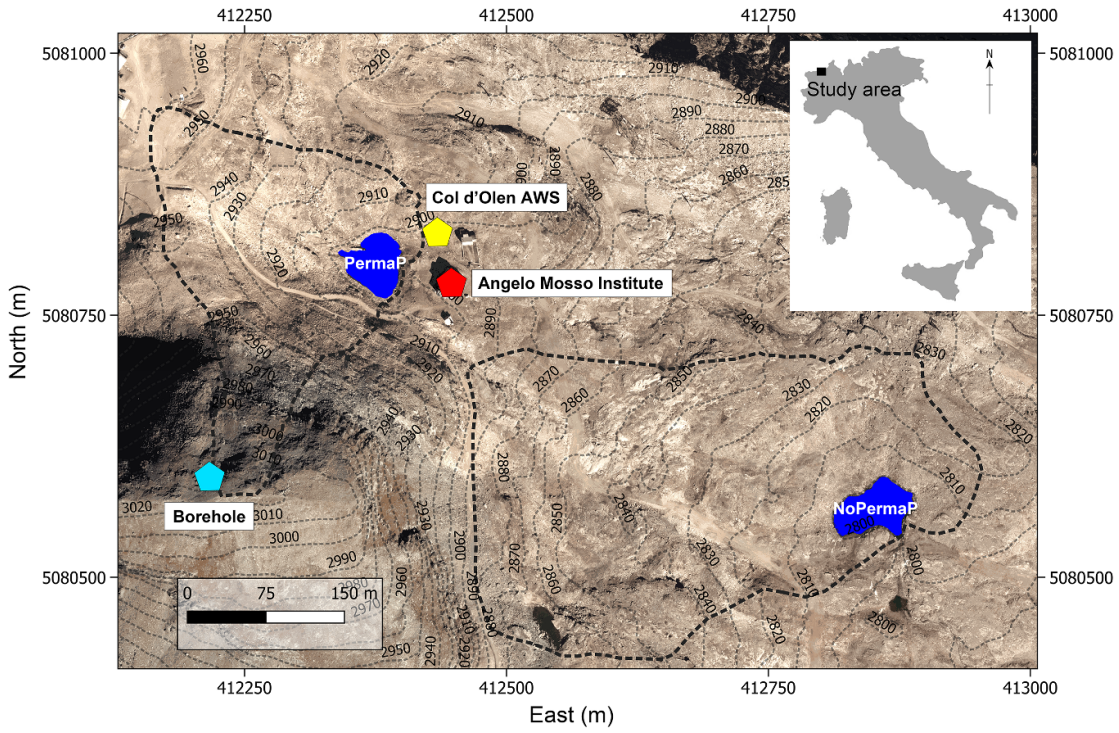

Figure 1. Location of the study area in Italy together with borders (dashed line) of the ponds' catchments (basemap: orthoimage AGEA, Piemonte Region, year 2018; coordinate reference system: WGS84 UTM zone 32 N). Col d'Olen AWS (yellow pentagon), 30-m deep borehole (cyan pentagon), and Angelo Mosso Scientific Institute (red pentagon) are also reported in the map. The Corno del Camoscio peak is located a few meters away from the borehole (3024 m a.s.l.). The NoPermaP catchment area differs from the one reported by Colombo *et al* [23] due to additional analyses performed thanks to new data availability and further field-site investigations; updated NoPermaP catchment area was already reported by Vione *et al* [24].

Table 1. Morphometric and land cover characteristics of the investigated ponds and catchments. We analyzed the morphometric characteristics using a 5 m × 5 m-cell digital elevation model-DEM (produced by Regione Piemonte). We mapped the land cover characteristics of the catchments by photointerpretation of digital orthoimages (years 2006–2021; sources: www.pcn.minambiente.it and www.geoportale.piemonte.it), supported by field surveys. morphometric and land cover characteristics differ from the ones reported by Colombo *et al* [23] due to additional analyses performed thanks to new data availability and further field-site investigations.

Feature	PermaP	NoPermaP
Pond elevation (m a.s.l.)	2900	2800
Pond area (m^2)	2300	2700
Pond maximum depth (m)	2.0	3.5
Catchment area (km^2)	0.05	0.11
Catchment mean elevation (m a.s.l.)	2938	2839
Catchment mean slope (°)	21	16
Catchment mean aspect (°)	80	116
Catchment land cover	Bedrock: 14 %	Bedrock: 31 %
	Coarse sediment: 68 %	Coarse sediment: 6 %
	Fine sediment/Soil: 14 %	Fine sediment/Soil: 60 %
	Water surface: 4 %	Water surface: 3 %

(supplement, text S4). We sampled the ponds from weekly (2015, 2018, 2019, 2020) to monthly (2014, 2016, 2017, 2021, 2022), usually between July and October (134 samples). Furthermore, we sampled rainwater on a weekly basis (2014, 2015, 2018, 2019, 2020; 43 samples), and we collected snow samples before snowpack melting began, in 2015, 2019, 2020, and 2021 (19 samples).

2.4. Stable water isotopes and mixing models

We determined the ratio of $^{18}O/^{16}O$ and $^{2}H/^{1}H$ of the collected water samples. Results are expressed as offset (δ per mil) from the Vienna standard mean ocean water. We analyzed the samples by means of cavity ring-down spectroscopy (CRDS Picarro L2130i). Analytical precision was below 0.25 ‰ and 1 ‰ for $\delta^{18}O$ and $\delta^{2}H$, respectively.

To identify the relative contribution from rainfall and snow to the recharge of the ponds (no groundwater springs are present in the catchments), we considered $\delta^{18}O$ as a tracer and used two types of mixing models. Firstly, we ran an end-member mixing analysis (EMMA) assuming the mixture (pond water samples) as a linear combination of the end-members (rainfall, snow). We assumed a time-invariant end-member signature. We used the mean and standard error values of the end-members' signatures to run the models and calculate their uncertainties based on Gaussian error propagation [28]. Secondly, we ran an ensembled end-member mixing analysis (EEMMA) [29]. This tool analyses the time series to estimate the contribution of the end-members to the mixture and can account for the presence of a memory-effect (i.e. no complete replacement of the end-member between samplings) and the potential occurrence of an unsampled end-member (supplement, text S5). Based on a DAS ordination, we built the EEMMA time series, and performed the models based on the entire dataset (all seasons), and separately between early season (DAS $<$ 35) and late season (DAS $\geqslant$ 35).

2.5. Chemical analyses

For the period 2014–2022, we determined the concentrations of SO_4^{2-}, NO_3^-, Cl^-, PO_4^{3-}, NO_2^-, Ca^{2+}, Mg^{2+}, Na^+, K^+, NH_4^+, Si, and dissolved organic carbon (DOC). We analyzed alkalinity in 2018, 2019, and 2020, while we analyzed HCO_3^- only in 2015. In the remaining years, we calculated alkalinity following Tosca and Tutolo [30]. Only in 2015, we analyzed Al and Fe. We also analyzed electrical conductivity (EC, at 20 °C) and pH (in laboratory). Analytical precision was: anions $<$10 %; cations, alkalinity, HCO_3^-, Si, Al, Fe, and DOC $<$5 %. Some analytes were analyzed by different laboratories (table S2, supplement, text S6).

2.6. Geochemical modeling and weathering proxies

We used the computer code PHREEQC V3 [31] and the phreeqc.dat and carbfix.dat databases [32] to calculate saturation indices (SIs) for various species: calcite, dolomite, gypsum, quartz, albite, anorthite, K-feldspar, k-mica, kaolinite, and allophane [33, 34] (supplement, text S7).

We applied a rate model consisting of reaction rates for pyrite (FeS_2) [35], anorthite ($CaAl_2Si_2O_8$) [36], and calcite ($CaCO_3$) [37, 38]. We adjusted the specific surface areas (SSAs) of pyrite, anorthite, and calcite to similar values in order to compare their relative dissolution kinetics between 0.3–5 m^2 mol^{-1}. We varied the available amount of pyrite between 5 and 50 mmol, and we ran the model for a duration of 120 d of the reaction at a water temperature of 9 °C to mimic natural conditions (supplement, text S7). Secondary phases which were allowed to precipitate were defined as $Fe(OH)_3(a)$, $SiO_2(a)$, and $Al(OH)_3(a)$. They represent the amorphous to poorly-crystalline Fe-(Hydr)oxides, Fe/Si-phases like hisingerite [34], and Al/Si-phases like allophane [33, 34] which control the level of Fe, Si, and Al, as observed in the measured data. In the rate model, we adjusted the SIs of the secondary phases to the average SI values, which were obtained by the thermodynamic calculation. Accordingly, the internal partial pressure of CO_2 (Pco_2) was set to $10^{-3.2}$ atm and to simulate oxidizing conditions we adjusted the Po_2 to atmospheric levels ($10^{-0.7}$ atm). Input parameters for the PHREEQC model can be found in table S3.

Finally, we used the S-ratio ($SO_4^{2-}/(SO_4^{2-} + HCO_3^-)$, in μeq L^{-1}) [39] to assess the dominance of sulfate (SO_4^{2-}; S-ratio = 1) versus hydrogen carbonate (HCO_3^-; S-ratio = 0) as a geochemical indicator for major weathering processes [cf. 20].

3. Results and discussion

3.1. Permafrost warming and thawing

MGTs significantly increased at all analyzed depths, with decadal warming rates ranging from 0.27 to 1.17 °C dec^{-1} (figure 2), consistent with those reported for the European mountains [40]. At all depths, MGT shifted from negative to positive values, indicating the thawing of permafrost. Our results are coherent with the ones reported by previous studies, which showed permafrost warming and thawing occurring across the globe [e.g. 1, 40], including the European Alps [e.g. 41, 42].

3.2. Similar water sources contribution, different solute concentrations in the ponds

EEMMA showed a similar partition of water sources feeding the ponds, with snowmelt contributing slightly more in PermaP (29 $\pm$ 21 %, $p < 0.05$) with respect to NoPermaP (26 $\pm$ 13 %, $p < 0.05$; table 2). During the early season, snowmelt contribution was moderately higher in PermaP (48 $\pm$ 11 %, $p < 0.001$) with respect to NoPermaP (31 $\pm$ 22 %, not significant), whereas in the late season it was similar between the ponds, although not significant (20 $\pm$ 20 % PermaP, 18 $\pm$ 13 % NoPermaP). The models did not identify any unsampled end-member; however, they estimated a significant memory effect (table 2), indicating a carryover in the mixture from sources associated with previous sampling campaigns. This carryover is attributed to water retention time, which is estimated to range from a few weeks to two months depending on the sampling period (supplement, text S1).

Although the ponds had similar water sources contributions, the concentrations of most solutes were significantly higher ($p < 0.001$, Kruskal-Wallis test) in PermaP (figure 3, table S4). This was particularly evident for SO_4^{2-} which was, on average, 3.9 times more concentrated in PermaP than in NoPermaP, followed by Mg^{2+}, Ca^{2+}, Na^+, and Cl^- (2.4–2.1 times). We also found slightly

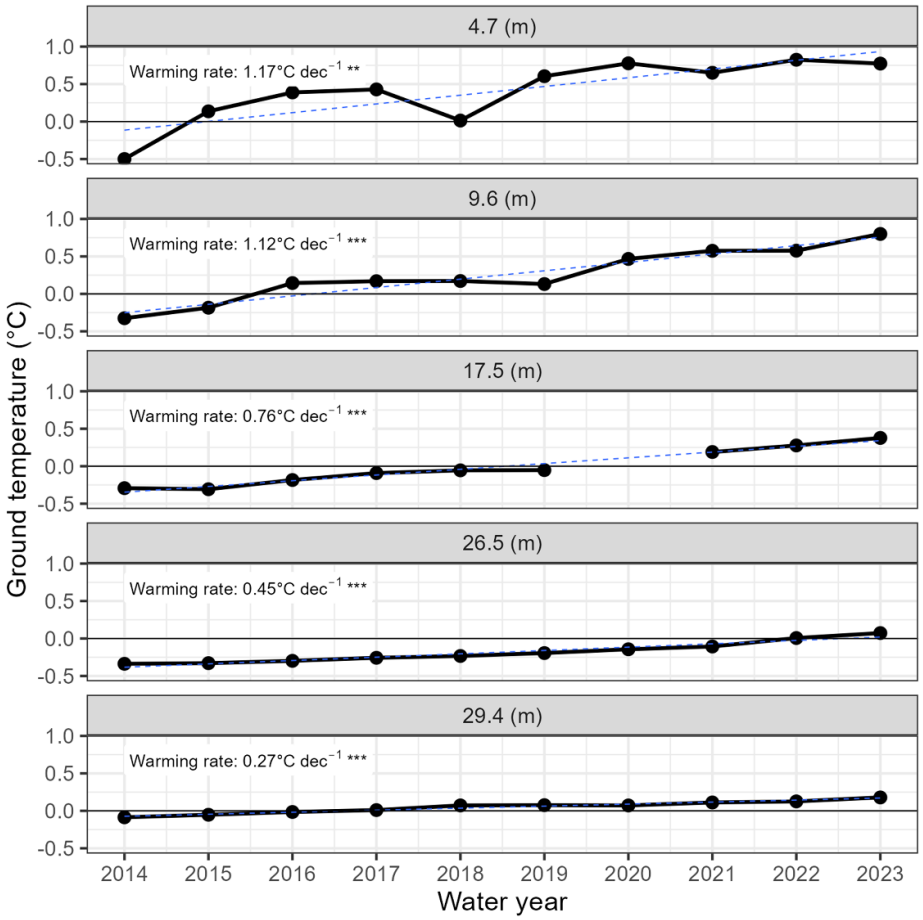

Figure 2. Mean ground temperature (MGT) trends and decadal warming rates at the five selected depths (4.7, 9.6, 17.5, 26.5, 29.4 m). We performed the MGT calculations based on the water year, 1 October−30 September (e.g. 2014 refers to the period encompassed between 1 October 2013 and 30 September 2014). * $p < 0.05$, ** $p < 0.01$, *** $p < 0.001$.

Table 2. Results obtained from the ensemble end-member mixing analysis (EEMMA). Early season (days after snowmelt − DAS < 35), late season (DAS ⩾ 35). Asterisks and 'ns' show the significance of the end-member contributions, the memory effect of the system, and the presence of an unsampled end-member. ns: not significant ($p > 0.05$), * $p < 0.05$, ** $p < 0.01$, *** $p < 0.001$.

End-members	PermaP (All seasons | Early season | Late season)	NoPermaP (All seasons | Early season | Late season)
Rain (%)	$71 \pm 21^{**}$ | $52 \pm 11^{***}$ | $80 \pm 20^{***}$	$74 \pm 13^{***}$ | $69 \pm 22^{**}$ | $82 \pm 13^{***}$
Snow (%)	$29 \pm 21^{*}$ | $48 \pm 11^{***}$ | 20 ± 20^{ns}	$26 \pm 13^{*}$ | 31 ± 22^{ns} | 18 ± 13^{ns}
Memory effect (%)	$82 \pm 15^{***}$ | $65 \pm 28^{*}$ | $70 \pm 24^{**}$	$69 \pm 17^{***}$ | $72 \pm 26^{**}$ | $50 \pm 27^{*}$
Unsampled (%)	ns | ns | ns	ns | ns | ns

higher concentrations of alkalinity and K^{+} (1.6–1.4 times). S-ratio was significantly higher in PermaP (0.54 ± 0.07) than in NoPermaP (0.34 ± 0.04). Si ($p = 0.82$) and DOC ($p = 0.32$) concentrations were not different between the two ponds.

The differences in most solute concentrations between the two ponds were little during the early season and increased toward the late season (table S4). This was particularly evident for SO_4^{2-} concentrations (figure 4(a)), showing the highest maximum increase in PermaP (up to 13.6 times) and a smaller increase (2.6 times) in NoPermaP, using DAS ordination and considering all years together (figure 4(b)). The outcomes from linear models (EMMA) further suggest that the contrasting SO_4^{2-} trends between the ponds were not related to a different dilution effect from snowmelt, since at similar estimated snow contributions, SO_4^{2-} concentrations between the ponds varied up to a factor of 9 (figure 4(c)). Dilution likely occurred in late spring−early summer, during the snow-melt peak, when solute-diluted snowmelt dominated the water inflow into the ponds (no samples are available for this period due to the ice cover on the ponds); this would explain the similar solute concentrations in both ponds at the beginning of the sampling season [see 26, 27].

The differences in solute concentrations were not caused by evaporation either, since all pond

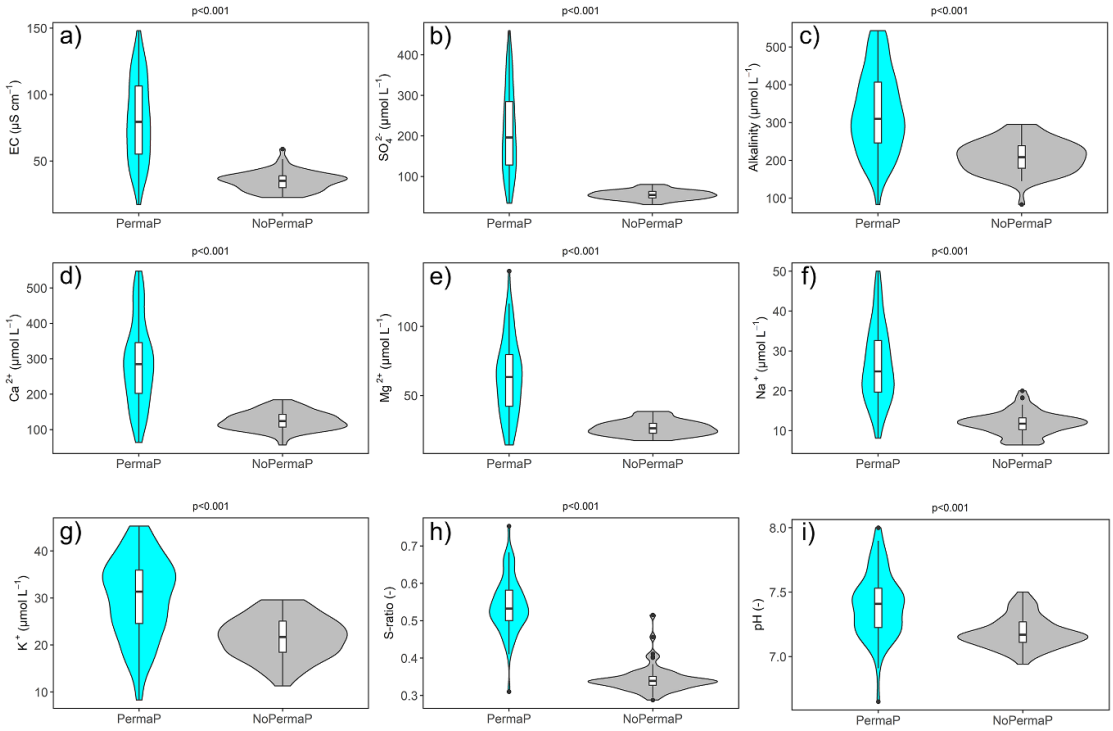

Figure 3. Violin plots of chemical variables. Significance levels (reported above each panel) result from the non-parametric Kruskal–Wallis test. Si, DOC, and Cl^- are not shown.

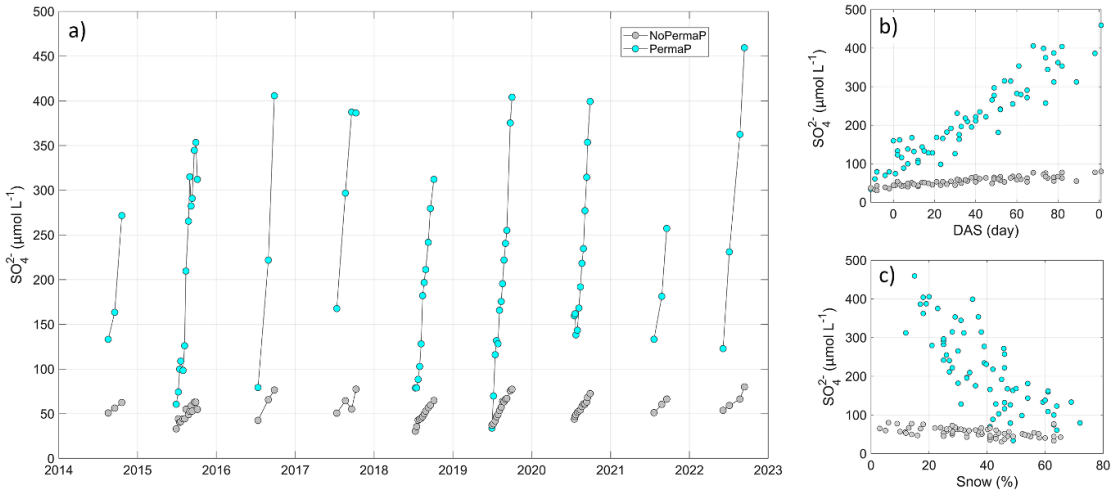

Figure 4. A) Time series of SO_4^{2-} concentrations at PermaP and NoPermaP. SO_4^{2-} concentrations vs b) days after snowmelt (DAS), c) snowmelt contributions estimated by end-member mixing analysis (EMMA; estimation uncertainty ranged from 4.8 to 8.3 %; mean ± standard deviation: 6.2 ± 0.8 %).

water samples aligned along the local meteoric water line in the dual isotope plot (figure S2) and exhibited deuterium excess [43] values (table S4, figure S3) not compatible with evaporative fractionation [44]. Therefore, we can exclude that the chemical differences between the two ponds were related to a different dilution from snowmelt water or to a different intensity of evaporative concentration [see 45, 46].

Finally, we ran generalized linear models and estimated the influence of DAS and Year covariates, as well as their interaction term, on the concentrations of SO_4^{2-} (response variable) in the PermaP and NoPermaP (two separate analyses; supplement, text S8). SO_4^{2-} concentrations were positively related to DAS in both PermaP and NoPermaP ($p < 0.001$), significantly related to Year only in PermaP ($p = 0.02$), and not significantly related to the interaction term of the two predictors (table S5). Therefore, while accounting for the time elapsed after the end of snow cover, SO_4^{2-} concentrations significantly increased during the investigated years, yet only in PermaP.

Based on these findings, we explored the chemical differences between the ponds by investigating the possible different weathering processes occurring in their catchments, as discussed below.

3.3. Enhanced weathering and sulfide oxidation from permafrost thawing

Potential sources of sulfate (SO_4^{2-}) include atmospheric deposition, decomposition of organic matter (OM), sulfate minerals such as gypsum or anhydrite, and sulfide minerals like pyrite. In the investigated ponds, atmospheric input can be excluded since SO_4^{2-} showed very low concentrations in precipitation [23, 47]. Moreover, the two ponds are in close proximity, and this would result in much more similar SO_4^{2-} concentrations than observed. Enhanced decomposition of OM in the PermaP catchment might cause increases in concentrations of SO_4^{2-} and base cations in pond water if these elements were bound to OM [cf. 48]. However, DOC concentrations were similar in the ponds (table S4). The weathering of sulfate minerals can be excluded as well, due to the low saturation index calculated for gypsum at both ponds (–2.9 at PermaP and −3.7 at NoPermaP, table S6). In addition, we found no evidence of gypsum presence in the area.

Therefore, we suggest that the main source for SO_4^{2-} was the weathering of sulfide minerals, that are present in the study area [23]. The water of both ponds would allow pyrite dissolution/oxidation indicated by the calculated SI values under oxygen-saturated ($10^{-0.7}$ atm) and oxygen-depleted (10^{-40} atm) conditions (table S6). At PermaP, mean S-ratio values of 0.49 ± 0.05 and 0.60 ± 0.05 (table S4) for the early and late season (maximum value 0.75), respectively, testify a relatively intense occurrence of sulfide oxidation [23, 49] and its increasing influence during the summertime, especially if compared to the low values and lack of seasonality at NoPermaP (early season 0.34 ± 0.04, late season 0.35 ± 0.03).

Enhanced sulfide oxidation in the PermaP catchment was likely caused by permafrost thawing, as also reported to occur in other permafrost settings across the globe [12, 21, 48, 50]. Indeed, permafrost together with ground ice can constitute impermeable layers acting as an aquitard [51, 52], (i) protecting against the oxidation of sulfides due to the lack of oxygen (anoxic conditions) owing to the isolation from active groundwater flow and the atmosphere, and (ii) hindering the dissolution of minerals in frozen rock/sediment material [11]. Permafrost thawing and ice melting would allow the opening of new water pathways enabling shallow oxygenated, low-mineralized groundwater to access deeper ground levels. Then, the freshly exposed sulfides present in fine-grained rock/soil material and on rock surfaces can be oxidized, resulting in increasing SO_4^{2-} concentrations in surface waters [11, 53].

Summertime increases of SO_4^{2-} and other major solutes at PermaP are consistent with the results of previous studies on waters influenced by transitional permafrost. Indeed, in case of thawing permafrost, the seasonal thaw of the active layer allows the seeping water to progressively access mineral phases that were previously frozen [12, 23, 27]. However, at PermaP, seasonal solute trends occurred also when permafrost had already mostly disappeared (at least within the borehole), for instance during the summer-fall 2022, when SO_4^{2-} concentration increased almost four times (from 123 μmol L^{-1} at the beginning of June to 459 μmol L^{-1} in mid-September). Therefore, we hypothesize that solute seasonality in transitional or recent permafrost-free catchments, richer in fresh mineral surfaces at depth, might persist due to the evolution of the flow paths during the thawing of the seasonally frozen ground. This process might influence water chemistry until the weathering-prone mineral surfaces that were recently exposed under permafrost thaw will be mostly exhausted, although the time scale of this phenomenon is currently unknown [11]; for instance, the full weathering of available pyrite could take hundreds to thousands of years [54]. In addition, areas with permafrost might still be preserved in the PermaP catchment, which is covered by coarse debris that favors ground cooling mechanisms [e.g. 55, 56].

The bedrock and fine-grained material in the catchment of both ponds are composed of a mixture of sulfides, silicates, and a small amount of carbonates [23], which explains the calculated SI values (table S6). The low SI values for calcite and dolomite at both ponds (between −5.7 and −1.9, table S6, supplement, text S9) suggest a similarly little influence of carbonate minerals, likely due to their low abundance. Indeed, their fast reaction kinetics [37, 38] would lead to a fast equilibration with the pond water, resulting in SI values close to 0, if carbonates were abundant. Moreover, both catchments are mostly composed of silicate rocks, having relatively slow reaction kinetics [36], especially at circumneutral pH conditions like those found in our systems. This is reflected in the low SI-values observed for albite, anorthite, and K-feldspar (between −4.8 and −8.1). Based on that, we applied a kinetic dissolution model by using rate laws for pyrite, anorthite (representing the silicates), and calcite.

We fitted the trend observed for the PermaP values by adjusting the amount of pyrite and calcite and the SSA of anorthite for the reaction time of 120 d, to mimic the duration of the snow-free season (figure 5, table S3). Variations in the amounts of pyrite, calcite, as well as changes in the SSA of anorthite resulted in different trends of EC, pH, and S-ratio during the reaction time. However, none of the variations

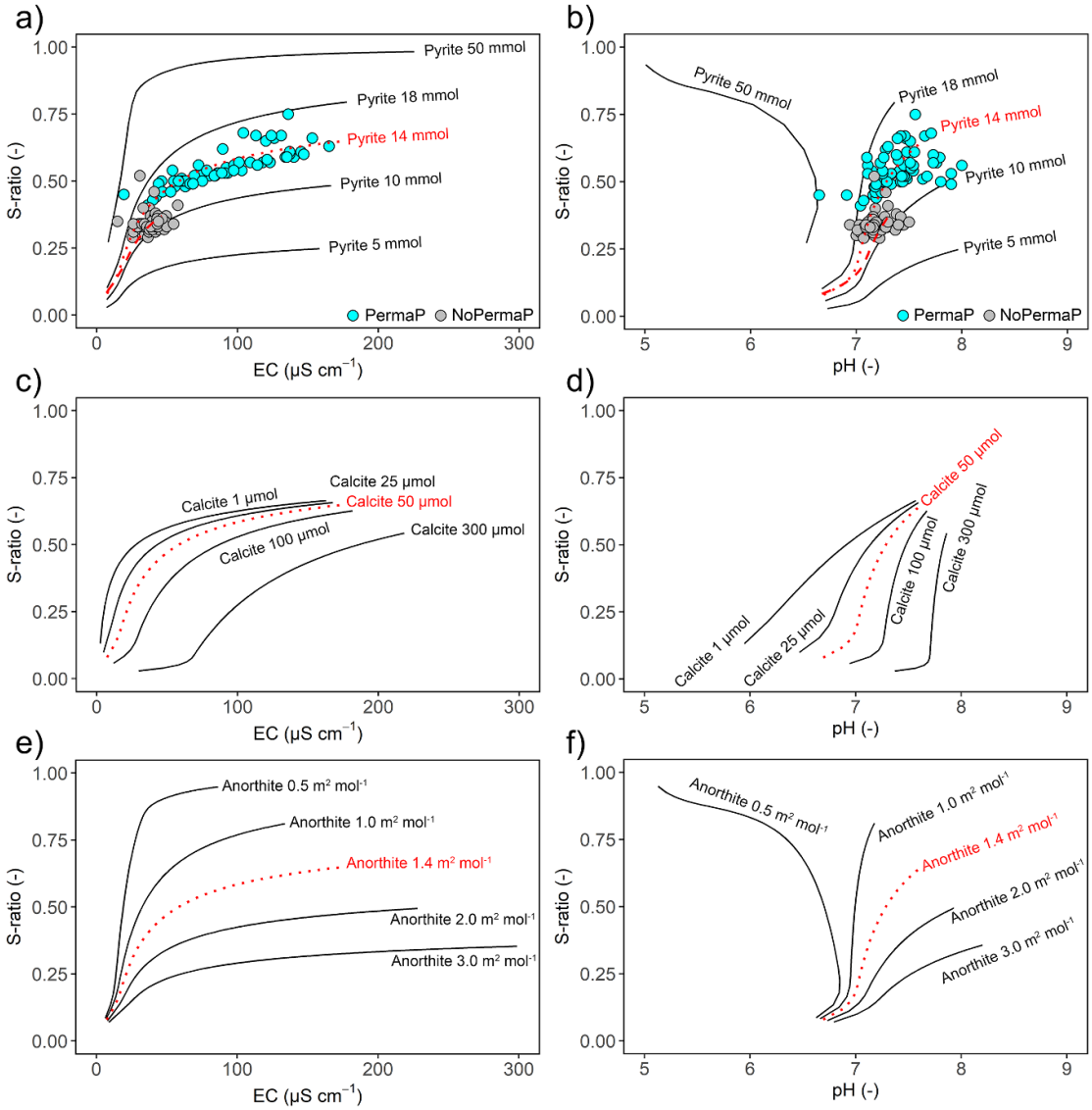

Figure 5. Diagrams showing the relationship between S-ratio and (a) electrical conductivity (EC) and (b) pH at PermaP and NoPermaP. Black lines depict the kinetic dissolution model of the chosen mineral assemblage with varying amounts of pyrite (a,b), calcite (c,d) and by varying the specific surface area of anorthite (e,f) with a reaction time of 120 d at a water temperature of 9 °C. Dotted red line shows the kinetic reaction fitted to the PermaP samples. Dashed red line shows the fit for NoPermaP values, which was obtained by reducing the reactive surface area of the mineral assemblage as well as reducing the amount of pyrite.

were able to replicate the trend observed for the NoPermaP samples. Only by reducing the SSA of all three components (pyrite, anorthite, and calcite) and by reducing the pyrite content, it was possible to reproduce the NoPermaP trend while maintaining the reaction time unaltered (figure 5(a) and (b), table S3).

Accordingly, in the PermaP catchment, the freshly exposed material surfaces dissolved relatively fast due to their high SSA and the supply of dissolved oxygen, despite the slow reaction kinetics of the silicate minerals (figure 6). The release of protons from pyrite oxidation subsequently increased the weathering intensity. Consequently, cation concentrations increased in the PermaP pond water but without any pH drop due to the buffering exerted by fine-grained and freshly exposed silicate minerals (figure 5). In contrast, in the NoPermaP catchment, the release of solutes was restricted by (i) the slow reaction kinetics of silicate weathering, but most importantly (ii) by the lack of freshly exposed rock particles (including sulfides) and of the related availability of reactive surface area (figures 5 and 6).

3.4. Sulfide oxidation may affect water quality

In this study, despite the prevalence of sulfide oxidation among weathering processes, pH was mostly above 7 and acidity-related elements such as Al and Fe (table S4) as well as Ni, Co, and Mn [23] had very low concentrations. Increasing sulfide oxidation due to permafrost thaw has been reported to degrade water quality through acidification and enhanced release of heavy metals from host rocks, following a process called natural acid rock drainage [13, 14]. Although

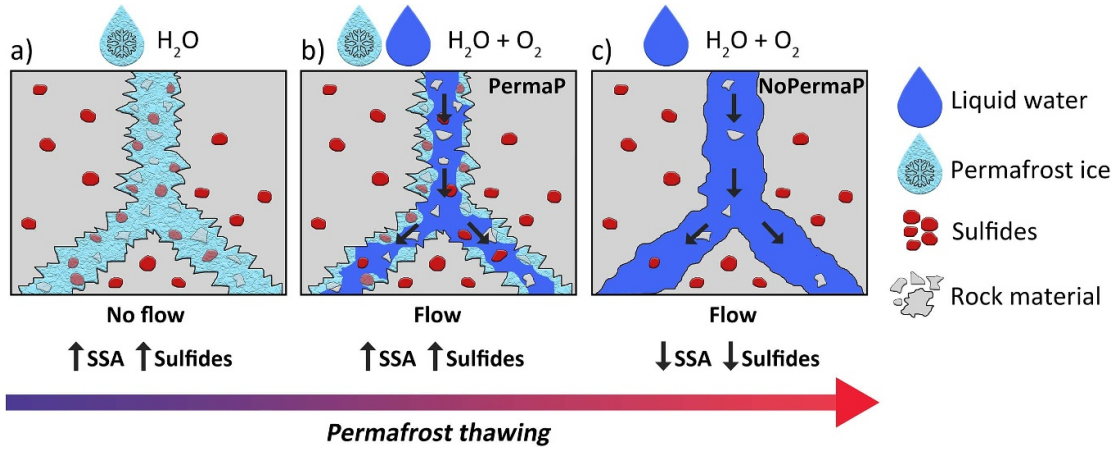

Figure 6. Conceptual model of the main weathering processes occurring in different phases of transitional permafrost conditions. (a) Intact permafrost conditions. Permafrost and ground ice constitute impermeable layers protecting against the oxidation of sulfides and hindering the dissolution of minerals ('No-flow' conditions). (b) PermaP conditions. Permafrost thawing and ice melting allow the opening of new water pathways enabling shallow groundwater to access deeper ground levels ('Flow' conditions). Then, the freshly exposed material surfaces dissolve relatively fast due to their high specific surface area (SSA) and the supply of dissolved oxygen. Enhanced sulfide oxidation causes sulfate concentration increase; pH is buffered by the presence of fine-grained and freshly exposed silicate minerals ('Rock material') and by carbonate dissolution (not shown because having little influence in our system). (c) NoPermaP conditions. The lack of freshly exposed rock particles (low SSA and sulfides) and the slow reaction kinetics of silicate weathering limit the release of sulfate and other solutes in the pond water.

the oxidation of Fe-sulfides like pyrite typically generates sulfuric acid, no significant pH decrease was observed at PermaP in the model experiment. We attribute this to the pH buffering capacity of dissolving silicates (and carbonates). In the reaction containing 5–18 mmol of pyrite, S-ratio and EC increased (figure 5(a)) as well as pH (figure 5(b)). Only if the relative available amount and/or the relative dissolution/oxidation rates of the Fe-sulfides versus the silicate (and carbonate) material exceeds some threshold, pH decreases, which is the case for the model using 50 mmol of pyrite (figure 5, supplement, text S10). Once the pH is lowered, the dominant oxidation mechanism shifts from dissolved oxygen to oxidation by ferric iron [57, 58].

To further confirm the role of sulfide oxidation and silicate/carbonate buffering capacity, we compared pH and S-ratio values of our ponds with the ones reported by Brighenti *et al* [20] for 201 springs from rock glaciers across different mountain ranges in the world. The authors found that (transitional) permafrost presence in these landforms enhances sulfide oxidation and the related export of solutes, yet under predisposing lithological settings (acidic metamorphic rocks such as paragneisses). In figure 7 we show that, at NoPermaP, values of pH and S-ratio align with those of springs from relict rock glaciers (i.e. without permafrost), whereas PermaP values are more coherent with those of intact rock glacier springs (influenced by permafrost). Thus, although at PermaP enhanced sulfide oxidation influenced the water chemistry with respect to NoPermaP, acidification was prevented by the relatively small amount of Fe-sulfides and the weathering of silicates and (small amount) of carbonates that was able to buffer the pH. In turn, this limited the release of heavy metals, thus preserving good water quality conditions. This hypothesis is corroborated by the above-mentioned study and by an additional work on a mountain river network draining acidic metamorphic rocks [49], showing that only S-ratio values larger than 0.7 are associated with water acidification, resulting in increased heavy metals concentrations and water-quality deterioration.

3.5. Research limitations

Given the long-term nature of the research conducted at this remote, high-elevation site, the sampling frequency has been primarily determined by resource and personnel availability. Nevertheless, solute trends, particularly for sulfate (figure 4), are well captured by both weekly and monthly sampling, confirming the robustness of the experimental design. Moreover, our geochemical model is a fairly simple approach to simulate natural weathering processes. Limitations arise from the complexity of the soil-sediment-rock with its heterogeneous mineralogical composition as well as the relative amount and the SSA of the rock/soil material, and individual reaction kinetics of the minerals contained. Furthermore, the aquifer systems of the ponds may be very spatially heterogeneous in terms of seasonal and inter-annual water pathways, leading to variable oxidizing and reducing conditions and weathering susceptibility. Nevertheless, the hydrogeochemical model can show the boundary conditions of the system in terms of the buffering effect of pH, the evolution of the S-ratio, and the amount of total dissolved solids (measured by EC), which depend largely on the composition of

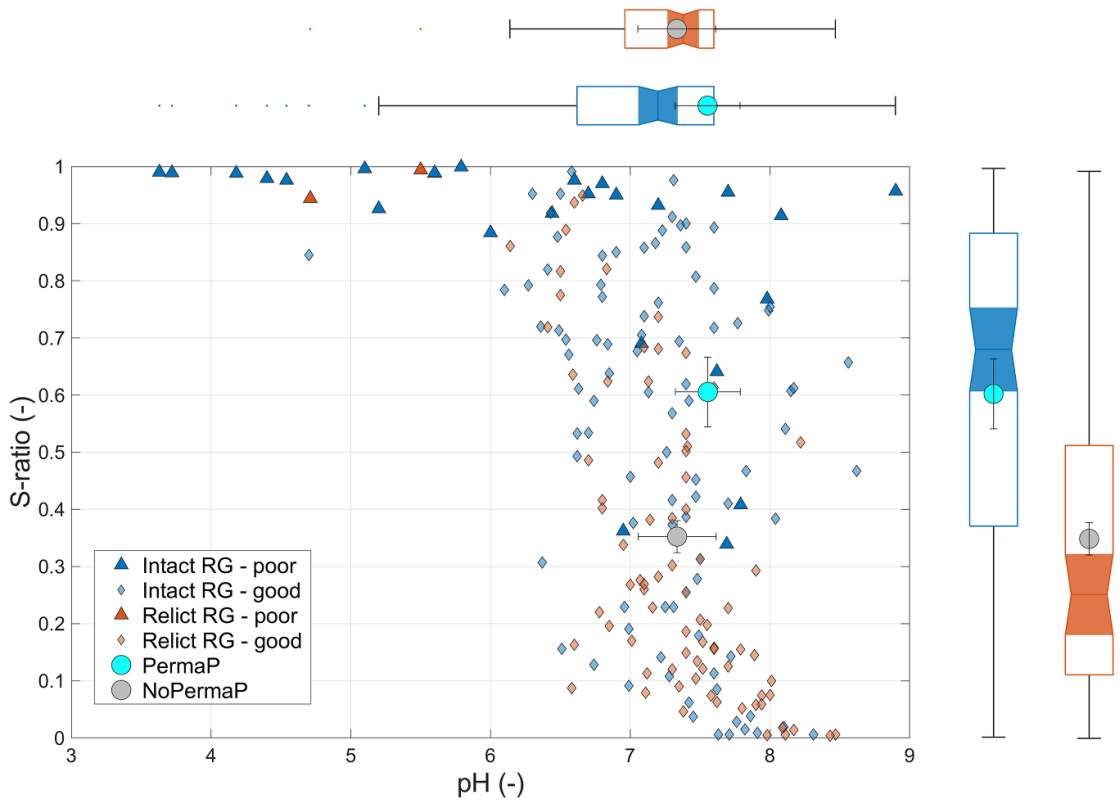

Figure 7. Comparison of PermaP and NoPermaP average values of pH versus S-ratio with the values of intact (Intact RG) and relict (Relict RG) rock glacier springs reported in Brighenti *et al* [20]. Poor (good) refers to RG samples with Ni, Al, Fe, Mn, and Zn exceeding (not exceeding) drinking water standard thresholds (good vs poor water quality). The box plots include all data for Intact RGs (blue) and Relict RGs (red), compared to PermaP (cyan dot) and NoPermaP (grey dot). To ensure consistency with the data reported by Brighenti *et al* [20], for the ponds we show only the average values associated with the highest EC during each year.

the rock/soil material. Therefore, while we acknowledge that site-specific conditions may limit the direct transferability of our findings to other settings, the underlying weathering processes and their interactions are likely relevant across a broad range of transitional permafrost environments, both in elevational and latitudinal contexts.

4. Conclusions

A growing body of research has documented the influence of permafrost thaw on water chemistry, primarily due to enhanced weathering of freshly exposed reactive minerals. In this study, we demonstrate that permafrost thaw also alters the chemical characteristics of high-mountain ponds in transitional permafrost environments. In particular, we identified sulfide oxidation as a major geochemical process resulting from thawing permafrost. While this process is often associated with acidification and deterioration of water quality in permafrost regions globally, our findings emphasize the critical role of the relative abundance and reaction rates of sulfides, silicates, and carbonates in buffering pH. As permafrost continues to warm and thaw at an accelerating pace, we anticipate that sulfide oxidation and chemical weathering will increase in transitional permafrost catchments. However, detrimental effects on water quality due to acidification are likely to occur only in catchments with specific lithological conditions, namely a large amount of fresh sulfide minerals and/or low acid-neutralizing potential of rocks. In such settings, ongoing deterioration of water quality is causing ecological modifications and, in some cases, the suspension of water withdrawals for human use. Our findings will support the assessment of potential future scenarios and their implications for water resource management in mountain regions.

Data availability statement

All data that support the findings of this study are included within the article (and any supplementary files). Raw data are available upon reasonable request from the authors.

Acknowledgments

We give special thanks to Stefania Vaccari and Lorena Masieri (Climate Change Unit, Environmental Protection Agency of Valle d'Aosta), Comando Truppe Alpine—Ufficio Meteomont (operating the Col d'Olen AWS), Environmental Protection

Agency of Piemonte Region (operating the 30-m ground temperature borehole), and Monterosa Spa and Monterosa 2000 (Monterosa ski). Stefano Brighenti was supported by the consortium iNEST (Interconnected North- East Innovation Ecosystem) funded by the European Union—Next Generation EU (PNRR) Missione 4 Componente 2, Investimento 1.5 D.D. 1058 23/06/2022, ECS_00000043). This work was funded by the European Union—NextGenerationEU, Mission 4 Component 2—ECS00000036—CUP [D17G22000150001].

Credit author statement

Nicola Colombo: Conceptualization, Investigation, Data Curation, Methodology, Software, Formal analysis, Visualization, Writing (original draft preparation, reviewing, and editing), Funding Acquisition. **Michael Pettauer:** Software, Formal analysis, Visualization, Writing (original draft preparation, reviewing, and editing). **Stefano Brighenti:** Data Curation, Software, Formal analysis, Writing (original draft preparation, reviewing, and editing). **Danilo Godone:** Investigation, Data Curation, Software, Formal analysis, Visualization, Writing (original draft preparation, reviewing, and editing). **Franco Salerno:** Investigation, Data Curation, Writing (reviewing and editing). **Raffaella Balestrini:** Investigation, Data Curation, Writing (reviewing and editing). **Carlo Andrea Delconte:** Data Curation, Writing (reviewing and editing). **Emanuele Pintaldi:** Data Curation, Writing (reviewing and editing). **Andrea Benech:** Data Curation, Writing (reviewing and editing). **Luca Paro:** Investigation, Data Curation, Writing (reviewing and editing). **Maria Martin:** Data Curation, Writing (reviewing and editing). **Alessandra Brunier:** Data Curation, Writing (reviewing and editing). **Nicolas Guyennon:** Formal analysis, Writing (reviewing and editing). **Michele Freppaz:** Investigation, Writing (reviewing and editing), Funding Acquisition.

ORCID iDs

N Colombo 0000-0003-2244-3147
M Pettauer 0000-0003-4383-3945
S Brighenti 0000-0001-6111-2311
D Godone 0000-0003-1455-6862
F Salerno 0000-0002-3419-6780
E Pintaldi 0000-0001-8345-4283
A Benech 0009-0004-5877-863X
L Paro 0009-0009-8326-4936
M Martin 0000-0003-1075-7739
N Guyennon 0000-0002-0306-0610
M Freppaz 0000-0002-4290-6850

References

[1] Biskaborn B K *et al* 2019 Permafrost is warming at a global scale *Nat. Commun.* **10** 264
[2] Smith S L *et al* 2022 The changing thermal state of permafrost *Nat. Rev. Earth Environ.* **3** 10–23
[3] Liu Z *et al* 2024 Widespread deepening of the active layer in northern permafrost regions from 2003 to 2020 *Environ. Res. Lett.* **19** 014020
[4] Gudmundsson L, Kirchner J, Gädeke A, Noetzli J and Biskaborn B K 2022 Attributing observed permafrost warming in the northern hemisphere to anthropogenic climate change *Environ. Res. Lett.* **17** 095014
[5] IPCC 2019 *IPCC Special Report on the Ocean and Cryosphere in a Changing Climate* ed H O Pörtner *et al* (Cambridge University Press) (available at www.ipcc.ch/srocc/)
[6] Schuur E A *et al* 2015 Climate change and the permafrost carbon feedback *Nature* **520** 171–9
[7] Hjort J, Streletskiy D, Doré G, Wu Q, Bjella K and Luoto M 2022 Impacts of permafrost degradation on infrastructure *Nat. Rev. Earth Environ.* **3** 24–38
[8] Webb E E and Liljedahl A K 2023 Diminishing lake area across the northern permafrost zone *Nat. Geosci.* **16** 202–9
[9] Vonk J E *et al* 2015 Reviews and syntheses: effects of permafrost thaw on Arctic aquatic ecosystems *Biogeosciences* **12** 7129–67
[10] Frey K E and McClelland J W 2009 Impacts of permafrost degradation on arctic river biogeochemistry *Hydrol. Process.* **23** 169–82
[11] Colombo N, Salerno F, Gruber S, Freppaz M, Williams M, Fratianni S and Giardino M 2018 Review: impacts of permafrost degradation on inorganic chemistry of surface fresh water *Glob. Planet. Change.* **162** 69–83
[12] Kemeny P C *et al* 2023 Arctic permafrost thawing enhances sulfide oxidation *Glob. Biogeochem. Cycles* **37** e2022GB007644
[13] Wanner C, Moradi H, Ingold P, Cardenas Bocanegra M A, Mercurio R and Furrer G 2023 Rock glaciers in the Central Eastern Alps—how permafrost degradation can cause acid rock drainage, mobilisation of toxic elements and formation of basaluminite *Glob. Planet. Change* **227** 104180
[14] O'Donnell J A *et al* 2024 Metal mobilization from thawing permafrost to aquatic ecosystems is driving rusting of Arctic streams *Commun. Earth Environ.* **5** 268
[15] Gruber S, Hoelzle M and Haeberli W 2004 Permafrost thaw and destabilization of Alpine rock walls in the hot summer of 2003 *Geophys. Res. Lett.* **31** 13
[16] Courtial-Manent L, Ravanel L, Mugnier J-L, Deline P, Lhosmot A, Rabatel A, Duvillard P-A and Batoux P 2024 18-years of high-Alpine rock wall monitoring using terrestrial laser scanning at the Tour Ronde east face, Mont-Blanc massif *Environ. Res. Lett.* **19** 034037
[17] Marcer M, Cicoira A, Cusicanqui D, Bodin X, Echelard T, Obregon R and Schoeneich P 2021 Rock glaciers throughout the French Alps accelerated and destabilised since 1990 as air temperatures increased *Commun. Earth Environ.* **2** 81
[18] Kellerer-Pirklbauer A *et al* 2024 Acceleration and interannual variability of creep rates in mountain permafrost landforms (rock glacier velocities) in the European Alps in 1995–2022 *Environ. Res. Lett.* **19** 034022
[19] Thies H, Nickus U, Mair V, Tessadri R, Tait D, Thaler B and Psenner R 2007 Unexpected response of high Alpine Lake waters to climate warming *Environ. Sci. Technol.* **41** 7424–9
[20] Brighenti S *et al* 2024 Factors controlling the water quality of rock glacier springs in European and American mountain ranges *Sci. Total Environ.* **953** 175706
[21] Steingruber S M 2024 The influence of atmospheric deposition and climate change driven catchment internal processes on the recovery from acidification of high-altitude Alpine lakes *Sci. Total Environ.* **930** 172699

[22] Zhou H, Li Z, Zhang B, Du F and Xue J 2024 Sources and chemical weathering implications of strontium and hydrochemistry in an Inland Alpine Permafrost Basin *Geochem. Geophys. Geosyst.* **25** e2024GC011432
[23] Colombo N *et al* 2019 Influence of permafrost, rock and ice glaciers on chemistry of high-elevation ponds (NW Italian Alps) *Sci. Total Environ.* **685** 886–901
[24] Vione D *et al* 2021 Seasonal variations in the optical characteristics of dissolved organic matter in glacial pond water *Sci. Total Environ.* **759** 143464
[25] Colombo N, Gruber S, Martin M, Malandrino M, Magnani A, Godone D, Freppaz M, Fratianni S and Salerno F 2018 Rainfall as primary driver of discharge and solute export from rock glaciers: the col d'Olen rock glacier in the NW Italian Alps *Sci. Total Environ.* **639** 316–30
[26] Brighenti S, Engel M, Tolotti M, Bruno M C, Wharton G, Comiti F, Tirler W, Cerasino L and Bertoldi W 2021 Contrasting physical and chemical conditions of two rock glacier springs *Hydrol. Process.* **35** e14159
[27] Bearzot F *et al* 2023 Hydrological, thermal and chemical influence of an intact rock glacier discharge on mountain stream water *Sci. Total Environ.* **876** 162777
[28] Genereux D 1998 Quantifying uncertainty in tracer-based hydrograph separations *Water Resour. Res.* **34** 915–9
[29] Kirchner J W 2023 Mixing models with multiple, overlapping, or incomplete endmembers, quantified using time series of a single tracer *Geophys. Res. Lett.* **50** e2023GL104147
[30] Tosca N J and Tutolo B M 2023 Alkalinity in theory and practice *Elements* **19** 7–9
[31] Parkhurst D L and Appelo C A J 2013 Description of input and examples for PHREEQC version 3—a computer program for speciation, batch-reaction, one-dimensional transport, and inverse geochemical calculations *U.S. Geol. Surv. Tech. Methods* **6** 497 (available at https://pubs.usgs.gov/tm/06/a43/)
[32] Voigt M, Marieni C, Clark D E, Gíslason S R and Oelkers E H 2018 Evaluation and refinement of thermodynamic databases for mineral carbonation *Energy Procedia* **146** 81–91
[33] Su C and Harsh J B 1998 Dissolution of allophane as a thermodynamically unstable solid in the presence of boehmite at elevated temperatures and equilibrium vapor pressures *Soil Sci.* **163** 4299–312
[34] Baldermann A, Stamm F M, Farkaš J, Löhr S, Ratz B, Letofsky-Papst I and Dietzel M 2024 Precipitation of short-range order hydroxy aluminosilicate (HAS) and hydrous ferric silicate (HFS) at ambient temperature: insights into mineral formation pathways, crystal chemistry and solubility-stability relationships *Chem. Geol.* **646** 121911
[35] Williamson M A and Rimstidt J D 1994 The kinetics and electrochemical rate-determining step of aqueous pyrite oxidation *Geoch. Cosm. Act* **58** 5443–54
[36] Palandri J L and Kharaka Y K 2004 A compilation of rate parameters of water-mineral interaction kinetics for application to geochemical modeling *U.S. Geol. Surv.* 2004–1068
[37] Plummer L N, Wigley T M L and Parkhurst D L 1978 The kinetics of calcite dissolution in CO2-Water systems at 5 degrees to 60 degrees C and 0.0–1.0 Atm CO2 *Am. J. Sci.* **278** 179–216
[38] Appelo C A J and Postma D 2004 Geochemistry, groundwater and pollution (CRC Press)
[39] Tranter M, Sharp M J, Brown G H, Willis I C, Hubbard B P, Nielsen M K, Smart C C, Gordon S, Tulley M and Lamb H R 1997 Variability in the chemical composition of *in situ* subglacial meltwaters *Hydrol. Process.* **11** 59–77
[40] Noetzli J *et al* 2024 Enhanced warming of European mountain permafrost in the early 21st century *Nat. Commun.* **15** 10508
[41] Pogliotti P *et al* 2023 Warming permafrost in the western alps: a further evidence of elevation dependent warming? *Rev. Géogr. Alp.* **111** 2
[42] Morard S, Hilbich C, Mollaret C, Pellet C and Hauck C 2024 20-year permafrost evolution documented through petrophysical joint inversion, thermal and soil moisture data *Environ. Res. Lett.* **19** 074074
[43] Daansgard W 1964 Stable isotopes in precipitation *Tellus* **16** 463–8
[44] Sprenger M, Leistert H, Gimbel K and Weiler M 2016 Illuminating hydrological processes at the soil-vegetation-atmosphere interface with water stable isotopes *Rev. Geophys.* **54** 674–704
[45] Brighenti S, Engel M, Dinale R, Tirler W, Voto G and Comiti F 2023 Isotopic and chemical signatures of high mountain rivers in catchments with contrasting glacier and rock glacier cover *J. Hydrol.* **623** 129779
[46] Akers P D *et al* 2024 The pivotal role of evaporation in lake water isotopic variability across space and time in a high arctic periglacial landscape *Water Resour. Res.* 60 e2023WR036121
[47] Balestrini R, Diémoz H, Freppaz M, Delconte C A, Caschetto M and Matiatos I 2024 Nitrogen atmospheric deposition in a high-altitude alpine environment: a chemical and isotopic approach to investigate the influence from anthropized areas *Atmos. Environ.* **328** 120513
[48] Crawford J T, Hinckley E-L S, Litaor M I, Brahney J and Neff J C 2019 Evidence for accelerated weathering and sulfate export in high alpine environments *Environ. Res. Lett.* **14** 124092
[49] Brighenti S *et al* 2025 Increasing nickel concentrations in a large river network of south tyrol, eastern European Alps *ACS ES&T Water ACS EST Water* **5** 594–604
[50] Walsh E V, Hilton R G, Tank S E and Amos E 2024 Temperature sensitivity of the mineral permafrost feedback at the continental scale *Sci. Adv.* **10** 41
[51] Arenson L U, Harrington J S, Koenig C E M and Wainstein P A 2022 Mountain permafrost hydrology—A practical review following studies from the andes *Geosciences* **12** 48
[52] Pavoni M, Boaga J, Carrera A, Zuecco G, Carturan L and Zumiani M 2023 Brief communication: mountain permafrost acts as an aquitard during an infiltration experiment monitored with electrical resistivity tomography time-lapse measurements *Cryosphere* **17** 1601–7
[53] Manning A H, Petach T N, Runkel R L and McKnight D M 2024 Climate-driven increases in stream metal concentrations in mineralized watersheds throughout the Colorado Rocky Mountains, USA *Water Resour. Res.* **60** e2023WR036062
[54] Nordstrom D K 2009 Acid rock drainage and climate change *J. Geochem. Explor.* **100** 97–104
[55] Delaloye R and Lambiel C 2005 Evidence of winter ascending air circulation throughout talus slopes and rock glaciers situated in the lower belt of alpine discontinuous permafrost (Swiss Alps) *Nor. Geogr. Tidsskr.* **59** 194–203
[56] Wiegand T and Kneisel C 2024 Monitoring of thermal conditions and snow dynamics at periglacial block accumulations in a low mountain range in central Germany *Earth Surf. Process. Landf.* **49** 5321–38
[57] Nordstrom D K 1982 Aqueous pyrite oxidation and the consequent formation of secondary iron minerals *Acid Sulfate Weathering* **10** 37–56
[58] Holmes P R and Crundwell F K 2000 The kinetics of the oxidation of pyrite by ferric ions and dissolved oxygen: an electrochemical study *Geochim. Cosmochim. Acta* **64** 263–74